Oceanologia 64 (2022) 363—375

Available online at www.sciencedirect.com

ScienceDirect

journal homepage: www.journals.elsevier.com/oceanologia

ORIGINAL RESEARCH ARTICLE

Coastal upwelling by wind-driven forcing in the Caspian Sea: A numerical analysis

Fatemeh Fallah, Dariush Mansoury*

Faculty of Natural Resources and Marine Sciences, Tarbiat Modares University, Noor, Iran

Received 25 March 2021; accepted 18 January 2022
Available online 31 January 2022

KEYWORDS
Upwelling;
Vertical velocity;
Wind field;
Bottom topography;
Hydrodynamic modelling;
Caspian Sea

Abstract In this study, wind-driven coastal upwelling in the Caspian Sea was investigated using a developed three-dimensional hydrodynamic numerical model based on the Princeton Ocean Model (POM). The model was forced with wind fields and atmospheric fluxes from the ECMWF database and it considers freshwater inflows from the Volga, Kura and Ural Rivers. This model was implemented for 10 years (2008—2018). Findings indicated that the upwelling in the Caspian Sea was due to effects of wind and bottom topography, often occurring from May to September. In June and July, in the eastern part of the middle and sometimes southern basins, up to 3°C water temperature difference occurs between coastal and offshore areas. The vertical temperature gradient in the middle basin was larger than that in the southern basin. Upwelling in August in the eastern coasts of the middle basin within 25 km of coast from the depth of 15 m to the surface was shown, which was due to the effects of wind and bottom topography. In the middle basin, the highest vertical velocities caused by upwelling in June, July and August were 12, 13.82, and 10.36 m/day, respectively.

1. Introduction

Winds in specific areas lead to divergence of water mass in oceans and seas. If surface water is driven by wind action away from the coast, the only way for its replacement is by upwelling from below. Since there is a good chance that the upwelled water has been enriched in nutrients, an upwelling area is likely to be a site of enhanced biological production. Coastal upwelling is mainly influenced by winds and rotational effects of the Earth (Coriolis force), so that its formation is owing to the presence of coast as an impenetrable lateral boundary as well as the relatively shal-

* Corresponding autor at: Faculty of Natural Resources and Marine Sciences, Tarbiat Modares University, Noor, Iran.
E-mail addresses: fa.fallah1374@gmail.com (F. Fallah), mansoury@modares.ac.ir (D. Mansoury).
Peer review under the responsibility of the Institute of Oceanology of the Polish Academy of Sciences.

Production and hosting by Elsevier

https://doi.org/10.1016/j.oceano.2022.01.003

low waters of the continental shelf (Brink, 1983; Kämpf and Chapman, 2016). The denser mass of water rises to sea surface, so that the sea surface temperature drops. The horizontal movement of water masses toward the offshore decreases the sea level in the coastal area, and it creates a horizontal pressure gradient and produces a geostrophic current under Ekman's transfer function (Kämpf and Chapman, 2016). Many studies have related the coastline orientation and the upwelling-favorable winds (Anand et al., 2019; Closset et al., 2021; Li et al., 2018; Nigam et al., 2018; Sun et al., 2017; Wirasatriya et al., 2020). Owing to the prevailing wind regime in the summer, the formation of the upwelling phenomenon in the Caspian Sea is highly important (Ibrayev et al., 2010). The surface waters are often warmer during the summer in the shallow coastal areas of the Caspian Sea, while along the east coast of the middle and southern Caspian basins, due to favorable winds (parallel to the coast), the surface waters move toward the west coast, and create the this phenomenon in the east coast (Ibrayev et al., 2010). Furthermore, they sometimes cause downwelling on the west coast. Several factors, such as wind and bottom topography (length and curvature of the bed), affect the rise of water along the coast (Shanks et al., 2000). The bottom topography plays a key role in the formation of the long upwelling filaments, whose signature extends over the entire water column and influences the upper layer dynamics advecting water parcels offshore (Meunier et al., 2010). The upwelling phenomenon in warm seasons has an almost stable trend as confirmed in atmospheric (Kosarev and Yablonskaya, 1994) and satellite observations (Sur et al., 2000). During the summer, due to the prevailing north wind, a relatively strong current is generated from the eastern part of the sea to the center, creating the Ekman transport along the eastern part (Ibrayev et al., 2010). In July, the prevailing wind in the central Caspian Sea is often from north to south, causing the upwelling phenomenon on the east coast (Knysh et al., 2008), while in the winter, the movement of water mass to the south and north on the western and eastern parts, respectively, in the subsurface layer (up to 30 m depth) of the Caspian Sea creates a seasonal counterclockwise rotation (Gunduz and Özsoy, 2014). Sea surface temperature (SST) satellite data often show relatively colder waters along the coast and filaments penetrating offshore from the upwelling region. The upwelling region extends from 41° to 44°N along the eastern coast with a temperature anomaly of 2–3°C in a region extending 5–20 km from the coast (Gunduz and Özsoy, 2014). The thermohaline structures of the Caspian Sea waters in the areas near the river mouths as well as on the eastern shores of the middle Caspian basin, where upwelling is observed in the summer, have considerable inconsistency in three dimensions, and seasonal changes in the temperature and salinity of sea water are at 100 m and 20 m, respectively (Tuzhilkin and Kosarev, 2005). To investigate the upwelling phenomenon in the eastern coasts of the middle Caspian basin, one study used a three-dimensional COHERENS model whose horizontal model grid was 0.046 × 0.046 degree and, in the vertical direction, it had 30 layers in the sigma coordinates (Shiea and Bidokhti, 2015). The model was implemented for 5 years, and it was investigated by simulation results, studying the horizontal and vertical temperature structure, and velocities of the sea currents in

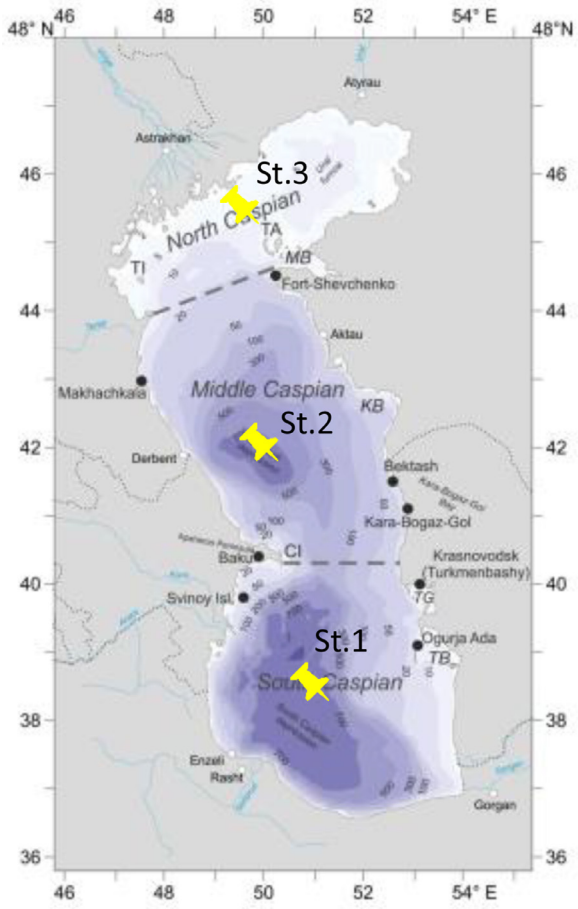

Figure 1 Three basins of the Caspian Sea.

the eastern area of the middle Caspian coast. The maximum vertical velocity was 12 m/day in July and 7 m/day in August (Shiea and Bidokhti, 2015; Shiea et al., 2016). Although previous research focused on studying the circulation of the Caspian Sea, some issues in simulation of the current field remain unresolved. Since currents over the Caspian Sea are primarily wind-driven (Ghaffari et al., 2013), their accurate simulations depend largely upon the wind data resolution (Kitazawa and Yang, 2012). However, to the best of our knowledge, previous studies did not apply well-resolved spatial changes of wind field over the Caspian Sea to predict its current field (e.g. Gunduz and Özsoy, 2014; Ibrayev et al., 2010; Turuncoglu et al., 2013). The major problem using satellite SST images to detect upwelling is that they only provide information about the near sea surface layer (Su and Pohlmann, 2009). In addition to the lack or scarcity of field measurements for the Caspian Sea, a high-resolution hydrodynamic model of the Southern Caspian Sea circulation is also absent in the literature. In this research, upwelling caused by wind and bottom topography during the year and in the whole Caspian Sea by applying more forcing and resolution (compared to previous research), was carried out using Princeton Ocean Model (POM). The purposes of the paper are (1) to implement the 3D hydrodynamic model (POM) for current, salinity and temperature fields modeling of the Caspian Sea by applying a 0.041° resolution; (2) to investigate the frequency of up-

Table 1 Main characteristics of the Caspian Sea (Arpe et al., 2018; Hall, 2002; Kostianoy and Kosarev, 2005).

Surface area (km^2)	North	386,400 in 2017	112,056
	Middle		139,104
	South		135,240
Volume (km^3)	North 1%	78,200	900
	South 66%		27335
	South 33%		49865
Length (km)		1,200	
Width (min-max) (km)		196-435	
Average depth (m)	North	5 (max 20)	
	Middle	190 (max 790)	
	South	330 (max 1025)	
Average surface temperature (°C)	North	Winter: 0°C with ice cover	Summer: 24
	South	Winter: 10	Summer: 27
Average surface salinity (psu)	North	4	
	Middle	12.8	
	South	13	

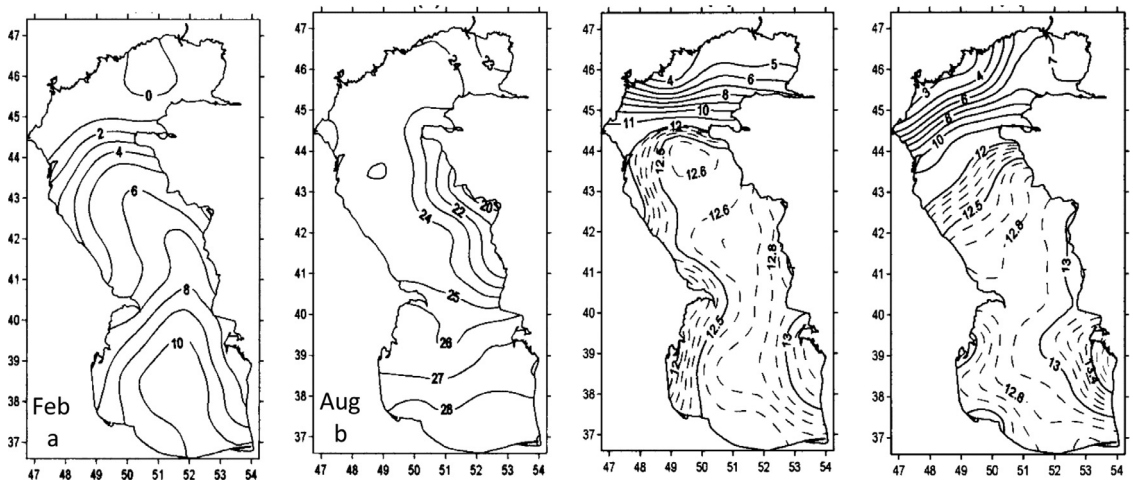

Figure 2 Climatic fields of the water temperature (°C, a, b) and salinity (psu, c, d) in the surface layer of the Caspian Sea in February and August (Tuzhilkin and Kosarev, 2005).

welling (per month) in the Caspian Sea using POM model; (3) In particular, we try to identify the roles of bottom topography and wind field as important upwelling mechanisms in the Caspian Sea.

2. General features of the Caspian Sea

2.1. Study area

The Caspian Sea, a landlocked body of water between Asia and Europe, and the largest enclosed sea basin in the world is located at 36—48°N and 46—55°E, with 40—44% of the total lacustrine waters of the world (Dumont, 1998; Bohluly et al., 2018). According to physical and geographical conditions as well as the bottom topography, the Caspian Sea is divided into three basins (Figure 1, Table 1), North Caspian Basin (NCB), Middle Caspian Basin (MCB) and South Caspian Basin (SCB) (Tuzhilkin and Kosarev, 2005; Zereshkian and Mansoury, 2020).

2.2. The climatic temperature and salinity fields of the Caspian Sea

Based on the results of statistical and physical analyses of ship and coastal measurement data (Tuzhilkin and Kosarev, 2005), the winter surface temperature field is characterized by its significant increase from the north to the south (Figure 2a). Heat losses during the winter in the northern and southern Caspian basins reach approximately 700 MJ m^{-2} and 200 MJ m^{-2}, respectively. Water temperatures are approximately 3°C lower than those in the open sea at the same latitude (Tuzhilkin and Kosarev, 2005). The advection of the waters of the northern and southern Caspian basins affects the surface temperatures of the western and eastern boundaries of the Middle Caspian Sea. The maximum values of the winter surface temperatures in the Middle Caspian result from the advection of warm waters from the south to the north along its eastern boundaries. In the summer, the minimum temperature of the Caspian Sea is observed in part of its eastern coast, which could be due to a summertime upwelling. The high summertime recurrence of upwelling

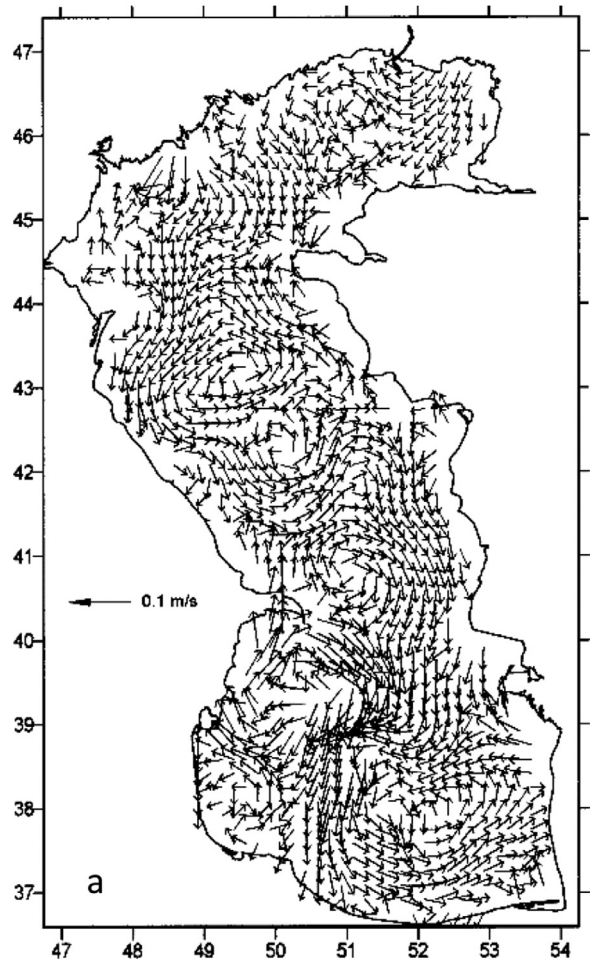

Figure 3 Annual mean climatic field of the current vectors in the surface layer of the Caspian Sea (Tuzhilkin and Kosarev, 2005).

off the eastern coast of the Middle Caspian from May to September makes this phenomenon climatically significant and it is well illustrated in the multiannual mean monthly fields of the water temperature (Figure 2b).

The salinity field in the Caspian Sea is subject to certain seasonal changes owing to its geographical location, river inflow, evaporation (shallow-water zones off arid eastern coasts), and precipitation (Tuzhilkin and Kosarev, 2005). In winter, due to reduced evaporation, surface salinity is low in the central and southern Caspian basins (Figure 2c). The propagation of reduced salinity from the northern basin to the middle is negligible due to high evaporation in the summer (Figure 2d).

2.3. The mean annual field of the current and wind of the Caspian Sea

The mean annual current velocities at the centers of the sub-basin gyres are 0.05—0.10 m s^{-1} and reach 0.20 m s^{-1} at the interfaces of gyres with opposite vorticities (Figure 3). Wind-induced currents play a rather significant role in the sea surface layer (Table 2). The current variability is related to the synoptic variability of the direct wind impact (Medvedev et al., 2020).

3. Data and methods

3.1. POM model

The POM is a simple-to-run yet powerful ocean modeling code to simulate a wide-range of problems, from small-scale coastal processes to global ocean climate change (http://www.ccpo.odu.edu/POMWEB/; Mellor and Blumberg, 1985). Many international researchers have studied numerous applications of this model in the modeling field in oceans and seas in different parts of the world. This model was provided by Princeton University in New Jersey and was developed with the support of the Geophysical Fluid Dynamics Laboratory (GFDL) of the National Oceanic and Atmospheric Administration (NOAA) as well as the Princeton Dynamic Analysis Institute (Blumberg and Mellor, 1987). The message passing interface Princeton Ocean Model (mpiPOM) was developed by Advanced Taiwan Ocean Prediction (ATOP), and it was optimized for the needs and resources of the ATOP system (Oey et al., 2013). This model was developed for the Caspian Sea with modifications and various types of coding as mpiPOM_Caspian Sea (mpiPOM-CS).

3.2. Data preparation to implement the model

Unfortunately, most of the time, there are not sufficient reliable data for the study area due to the lack of field measurements. For the model input, temperature and salinity data of the World Ocean Atlas (Antonov et al., 2006) were used; despite high accuracy (1°), the data do not cover the entire Caspian Sea and an algorithm for extrapolation, in addition to interpolation on the grid, should be used (Mansoury et al., 2015). The General Bathymetric Chart of the Oceans (GEBCO) aims to provide the most authoritative, publicly available bathymetry data sets for the oceans and seas including the Caspian Sea. Atmospheric fluxes data, including wind, precipitation, evaporation, heat fluxes (sensible and latent), and short and long wave solar radiation were received from the ECMWF database with an accuracy of 0.125° and a 6-hour time step. The most important rivers entering the Caspian Sea are Volga (5 branches), Kura and Ural. The monthly average of Naval Research Laboratory (NRL) data was used for the data of the rivers (Table 3; Kara et al., 2010). In this research, the model was implemented for ten years (2008—2018), and the last year outputs of the model implementation were investigated. The model domain is 46.5—55°E and 36.5—47°N with a horizontal resolution of 0.041° (about 4 km) and 35 vertical layers in sigma coordinates. It uses external and internal time steps of 2s and 90s, respectively. To apply the parallel processing, four cores were considered with a computational grid of 135 × 103.

3.3. Stability and validation of the model

In the course of a year, salinity has almost a round cycle, but in the first years of the model, it does not have a clear trend. Its multi-year repetition during model execution indicates that the model is stable (and can also be true for temperature). In this study, salinity changes in the last years of the model implementation show rela-

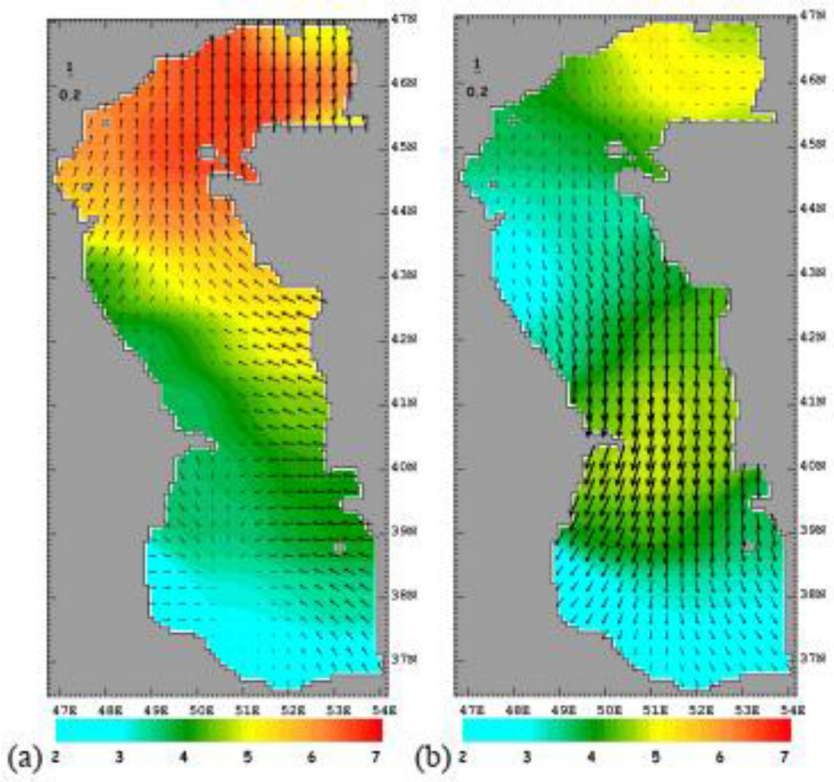

Figure 4 Monthly mean wind velocity vectors in (a) December and (b) July 1982. The units are in m/s (Ibrayev et al., 2010).

Table 2 Some wind features in the Caspian Sea (Ibrayev et al., 2010).

Wind speed (typically)	Summer (approximately 4 m/s) The maximum speed occurs to the east of the Apsheron Winter (approximately 5—6.5 m/s) The maximum speed occurs in the north (Figure 4a)
The classification of the annual cycle of the monthly mean wind	1 — December—January: With the convergence of winds in MCB and SCB due to high land-sea temperature (Figure 4a) 2 — February—July: When large-scale anti-cyclonic winds prevail over the sea (Figure 4b). 3 — August—November: When average wind direction gradually changes from south-, southwestward to westward.

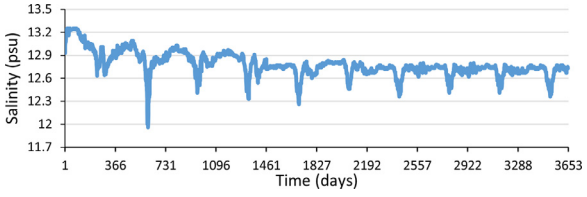

Figure 5 Changes in salinity in the ten-year implementation period of the model.

tively good model stability (Kämpf and Sadrinasab, 2006; Sadrinasab and Kämpf, 2004) (Figure 5).

The data collected during research cruises in the Caspian Sea in August and September (from 30.08.1996 for one week) were used to validate the model results. To validate the model output according to the available measurement data during 1996 (UNESCO-IHP-IOC-IAEA, 1996), the model was re-run for ten years (1988—1997). The results of the model output and measurements were compared to each other (Figure 6) in three positions (Figure 1).

The following comparisons indicate acceptable agreements between the model results and the measurement data and satellite image (https://oceancolor.gsfc.nasa.gov/). Due to the limited availability of the current velocity measurement data in the Caspian Sea, the mean annual current velocities of previous study (Figure 3), SST satellite image (Figure 7a) and this study (Figure 7b) were compared, showing good agreement between them.

3.4. Upwelling detection mechanism

Upwelling occurs due to divergence of currents in the surface layers of the sea caused by wind field, in the presence

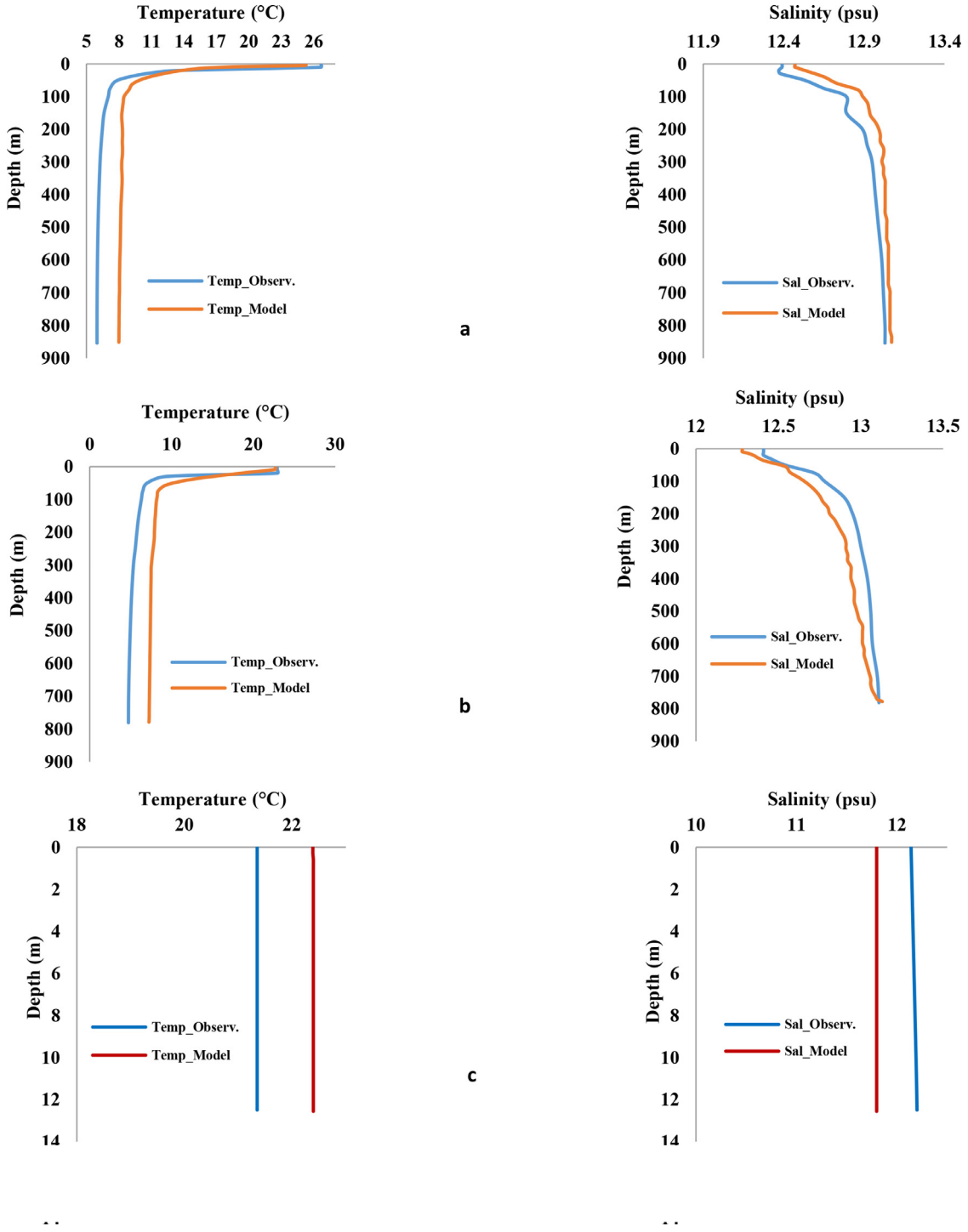

Figure 6 Comparison of modeled and observed temperature—salinity properties: a) St.1, b) St.2 and c) St.3 in 1996.

of the shoreline or other special conditions, after which the water of the lower layer (colder and denser) is transferred to the surface to maintain balance. The lower layers are known as permanent sources of nutrients, so productivity is significant in areas where upwelling occurs. Due to the favorable wind in the sea shores and the resulting ecumenical transfer, there is a difference in water level between the coast and offshore, and the pressure difference caused by them will follow the surface geostrophic flow. Changes in sea water temperature (surface temperature at nearshore and offshore, and the vertical section of seawater temperature) and sea currents (such as vertical velocity) due to a rise in a body of water from depth to surface which can be caused by wind and bottom topographic effects (Meunier et al., 2010), indicate the coastal upwelling (Ghaffari et al., 2013; Olita et al., 2013). In this research, owing to the physical and geographical location of the Caspian Sea, the Coriolis effect in differ-

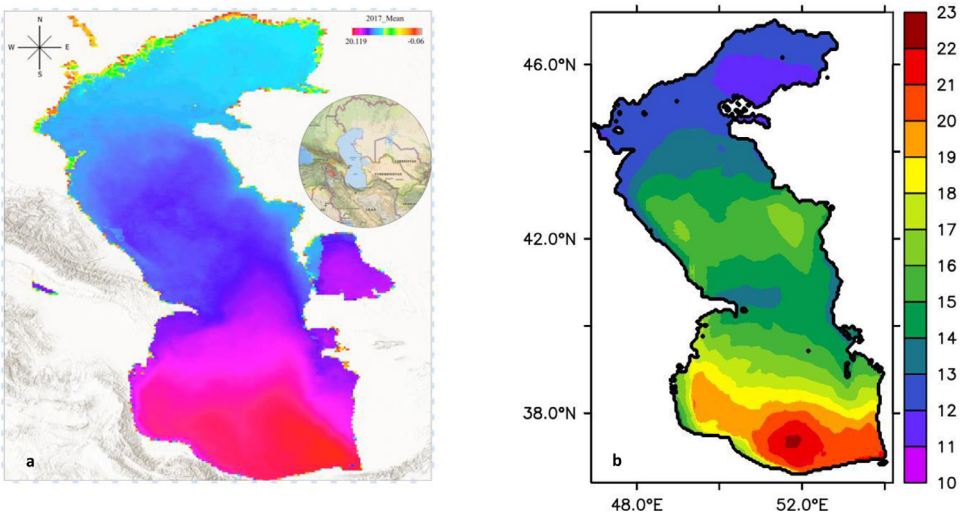

Figure 7 Annual mean climatic field of SST (°C): a) Satellite image (https://oceancolor.gsfc.nasa.gov/); b) Model output in the Caspian Sea.

Table 3 Monthly mean discharge for the major rivers discharged into the Caspian Sea (Kara et al., 2010).

	Volga (m^3/s)	Kura (m^3/s)	Ural (m^3/s)
January	780	490	50
February	790	500	55
March	800	530	60
April	1500	800	900
May	4780	1050	1370
June	4000	800	420
July	1650	450	220
August	1120	310	180
September	1000	315	140
October	1060	400	140
November	1070	420	135
December	780	460	80

Table 4 The maximum vertical velocities of seawater in upwelling events at 43°N in June.

Day	w_{max} (m/day)
11	10.5
12	11
13	10.1
27	10.3
28	11.3
29	12

Table 5 The maximum vertical velocities of seawater in upwelling events at 43°N in July.

Day	w_{max} (m/day)
22	12.09
24	8.64
25	13.82
26	7.77

Table 6 The maximum vertical velocities of seawater in upwelling events at 43°N in August.

Day	w_{max} (m/day)
3	10.36
4	6.04
5	6.9
6	8.64

ent latitudes and a variable wind field, as well as the ice effect were considered with an appropriate accuracy in mpiPOM-CS.

3. Results

3.1. Spatio-temporal variability of sea surface temperature

Figure 8 presents the monthly changes in the Caspian Sea temperature in 2017. In the northern and middle basins, the climate pattern is relatively cold and in the southern basin, the pattern is warm. Sea surface temperature from January to April in the three basins of the Caspian Sea have increased, and this increase in temperature in the northern basin (from January to April) is east-west due to depth changes (Figure 8a—d). These changes are caused by the lower depth of the eastern part compared to the western part of the basin and the lower heat capacity of the seafloor relative to seawater. The mean monthly seawater temperature in some parts of the Caspian Sea, particularly from May to September, undergoes unexpected changes (Figure 8e—i). SST changes in the eastern part of the middle and southern basins, from May to August and into part of September, are colder than offshore ones (blue ovals). From October to December, it resumes its natural trend (Figure 8j—l). In these months, the air temperature rises compared to previous months, and this increase in tem-

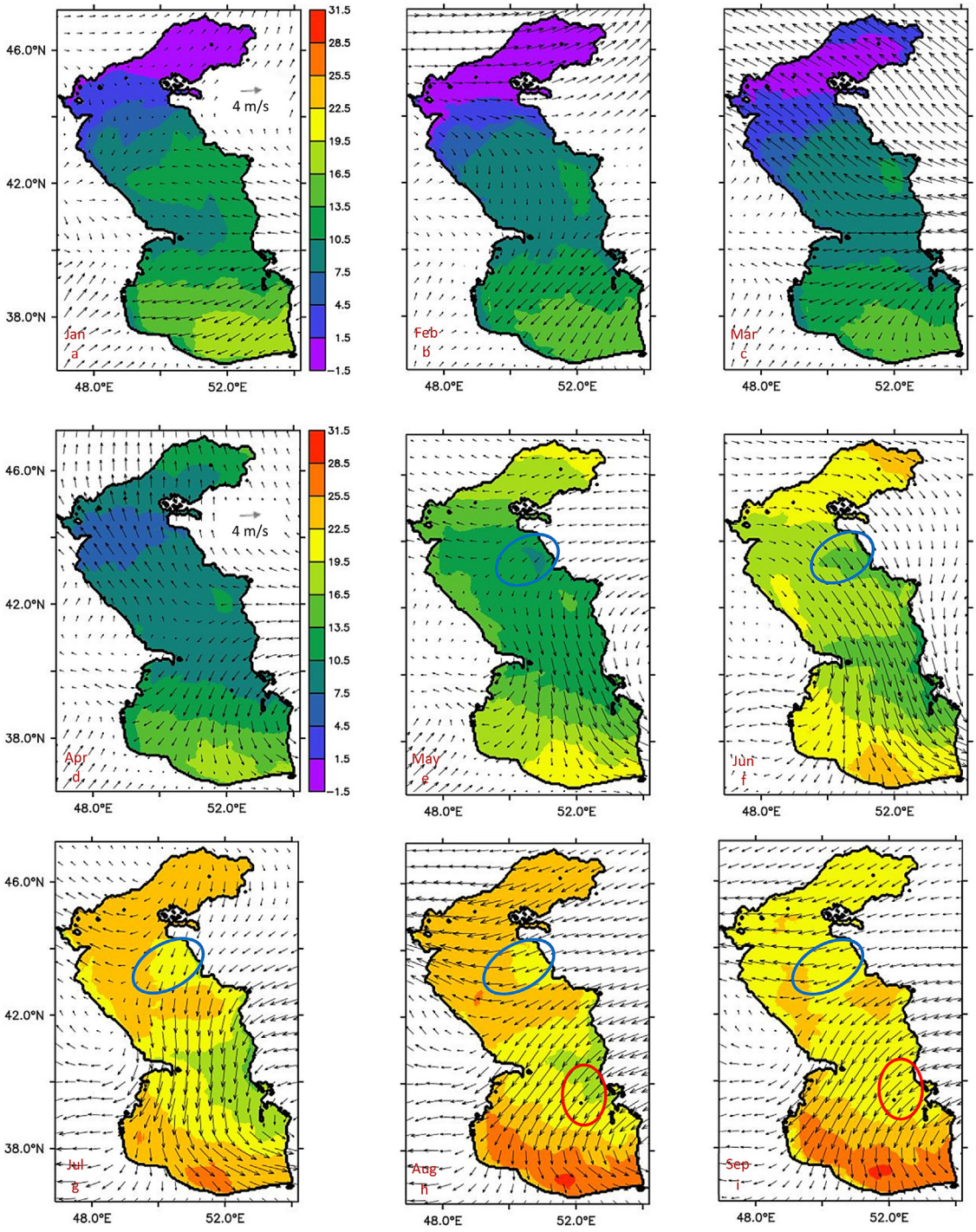

Figure 8 SST (°C) with monthly mean wind overlaid in 2017.

perature is expected to affect the eastern coasts of the Caspian Sea due to the shallow depth and to raise the surface temperature of the water. However, the sea surface water on the eastern shores of the central and southern Caspian basins has been colder compared to the offshore areas, which may be owed to the transfer of cold water from the lower layers to the sea level. The difference between the average sea surface temperature in the eastern part of the middle Caspian Basin (coastal and offshore) indicates the possibility of upwelling in these areas.

Nevertheless, the monthly pattern of the wind field in May, August and September does not show the Ekman transport in favor of upwelling (perpendicular to the coastline) (Figure 8e,h,i). However, the direction of the wind in this part, due to pushing the surface water, causes a difference in the water level between coastal and offshore areas, being consistent with the upwelling event. Since the effect of other factors (other than wind) may play a role in creating upwelling, it is necessary to examine the daily changes for a more detailed study. Northwest and north winds in

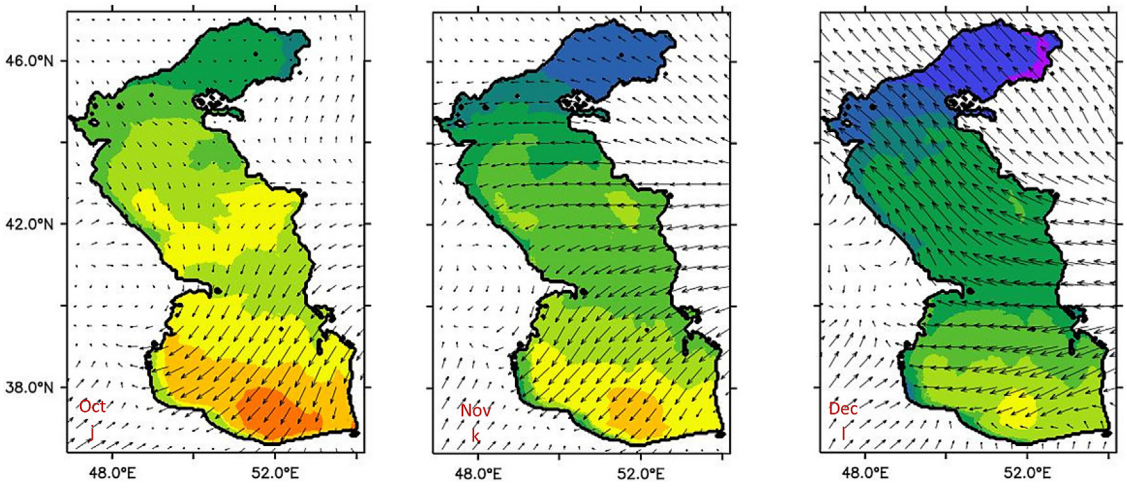

Figure 8 *Continued.*

June and July are the main mechanism of upwelling on the eastern coasts of middle and southern Caspian basins, owing to the Ekman transport perpendicular to the coastline (Figure 8f,g).

3.2. Vertical section of seawater temperature in middle and southern Caspian basins

In May, although the wind direction in the middle Caspian basin (at 43°N) is not parallel to the east coast (Figure 8e), a slight upwelling occurs in lower layers, which may be due to topographic effect (Figure 9a). However, in the southern Caspian basin (at 39°N), it is upwelling-favorable wind. Coastal upwelling is seen in the upper layers, which can be due to wind field effect (Figure 9b). In June, temperature contours show that the water masses of the eastern coasts of the middle and southern Caspian basins are the result of divergence of surface waters and the movement of water from lower layers to upper layers (Figure 9c,d). Wind field is the main factor of upwelling in this month (Figure 8f).The intensity of upwelling due to wind is higher in the middle basin than in the southern basin, so that the topographic effect in this basin is negligible (Figure 9). In July, in the middle basin, the rise of water mass at a depth of 20 m to the surface occurred, and in the southern basin at a depth of 12 m, partially along 52—53°E, according to the north wind (Figure 9e,f). Furthermore, in the middle basin, wind-driven upwelling is predominant.

In August and September, the rise of water mass from lower layers to upper layers in the middle basin (at 43 °N) can be seen in two parts (Figure 9h,i). The first part (blue ovals) indicates weak coastal upwelling considering the east and southeast wind and change at the coastal water level (Less than 10 m depth) (Figure 9g,i). However, the second parts (red ovals) show water rises from a depth of approximately 35 to 10 m (along another longitude), which can be due to sea currents encountering the seafloor (bottom topographic effect). Nevertheless, in the southern basin (at 39°N), rising water is seen only in part, at a depth of 35—10 m (orange ovals), which is similar to the middle basin owing to topographic effects (Figure 9h,j).

3.3. Monthly mean of vertical velocity in June and July

According to Figure 10, the maximum vertical velocity occurs at 51.2°E in June and July considering positive values.

3.4. Daily upwelling in June, July and August

Rising water mass from lower layers to the surface layer on June 27 (Figure 11a) in the longitude 51.2°E occurs considering the northwest wind that is almost parallel to the coastline (Figure 11b). Moreover, according to Table 4, the highest vertical velocity is estimated at 12 m/day in upwelling events this month, where w_{max} is the maximum vertical velocity.

On July 22, the water mass rises vertically in the longitude 51.20°E (Figure 12a,b), and according to Table 5, the highest vertical velocity is 13.82 m/day in upwelling events.

In August, according to the wind direction (southeast), the mechanism of formation of upwelling on the fourth day cannot be the effect of wind (Figure 13a). Although the vector of the wind field in this area is almost parallel to the coastline, its Ekman transport is to the onshore. Therefore, the formation of upwelling in this part of middle basin coasts can be due to topography (Figure 13b). The highest vertical velocity is 10.36 m/day in upwelling events (Figures 13b, 14, Table 6).

4. Conclusion

In this study, upwelling in the Caspian Sea was investigated using a developed three-dimensional hydrodynamic numerical model (mpiPOM-CS). The Validation of the model results based on measurement and observational data (satellite image) showed greater consistency of the simulation results. According to the findings, upwelling often occurs in the Caspian Sea from May to September, which is in good agreement with the results of studies conducted by Lavrova et al. (2011) and Tuzhilkin and Kosarev (2005) in the eastern part of the middle Caspian basin. The difference in SST between

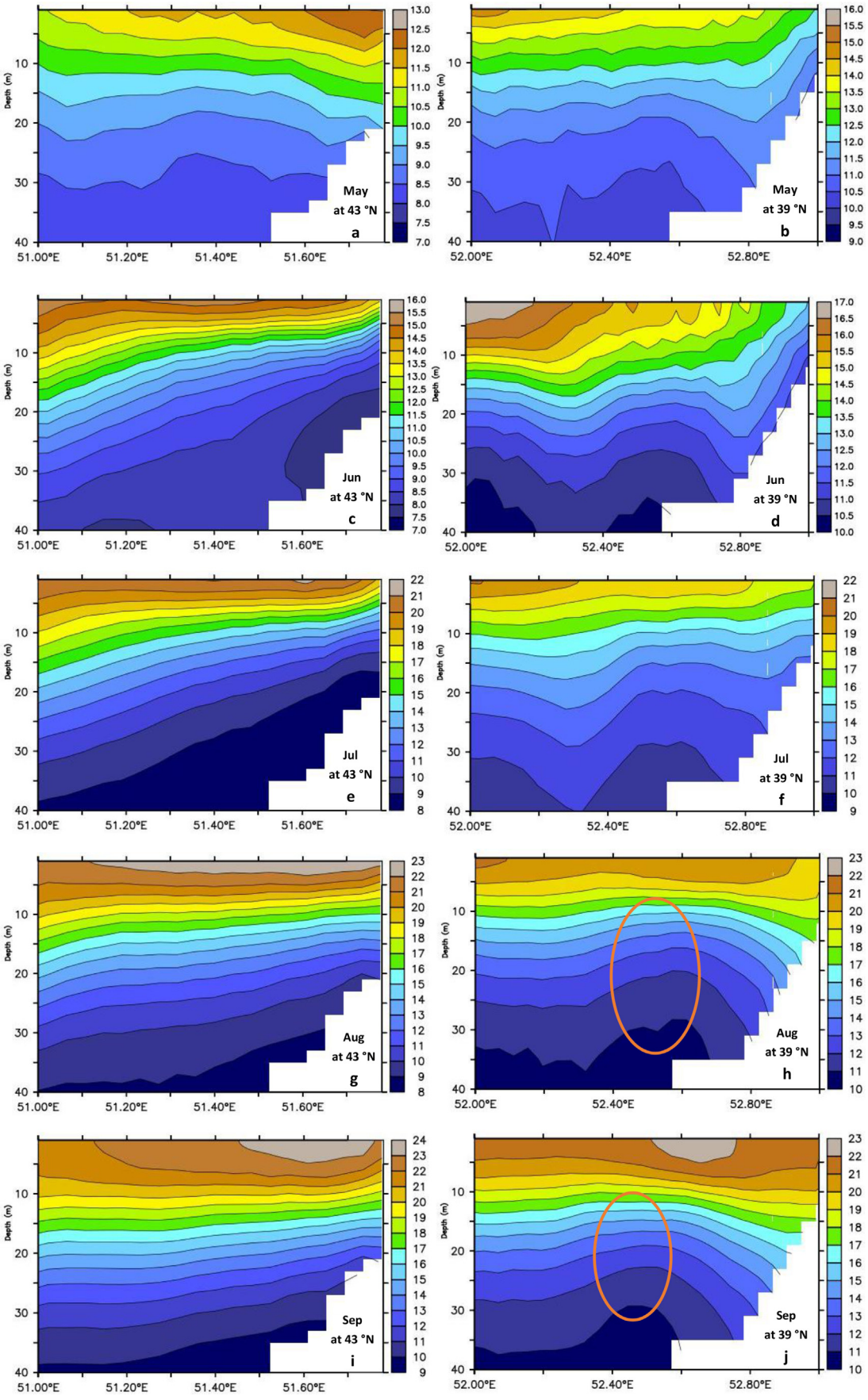

Figure 9 Vertical section of the seawater temperature (°C) in MCB and SCB (May—September).

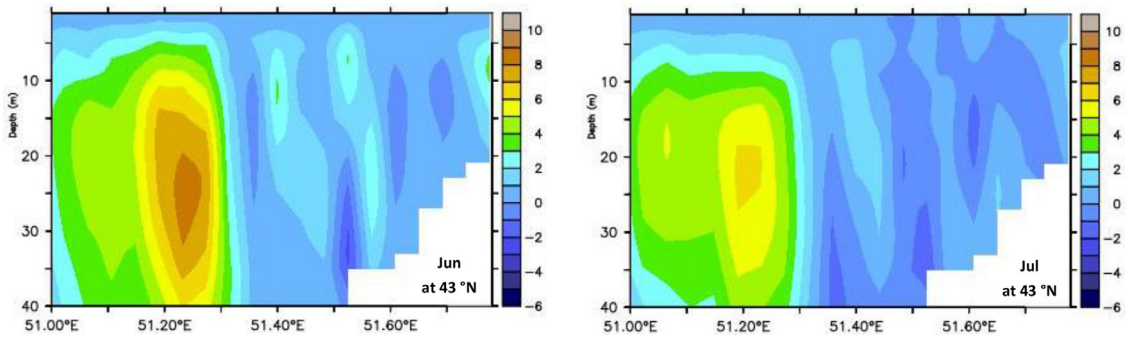

Figure 10 Monthly mean of the vertical velocity (m/day) in MCB.

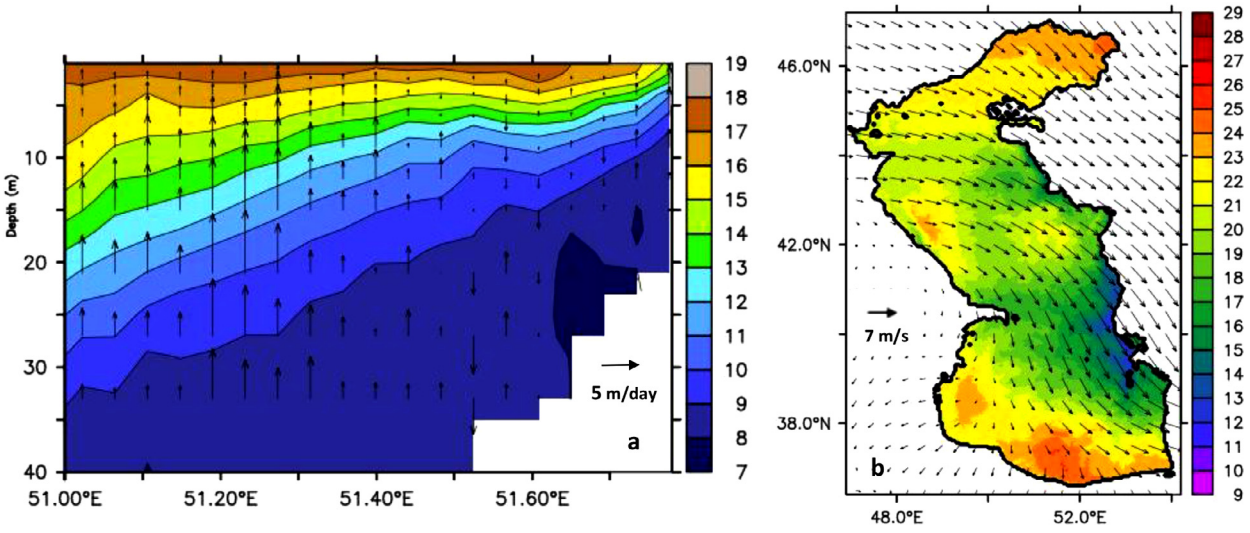

Figure 11 Vertical velocity over the vertical section of seawater temperature (°C) at 43°N (a) and SST (°C) with wind field overlaid (b) in the Caspian Sea on June 27.

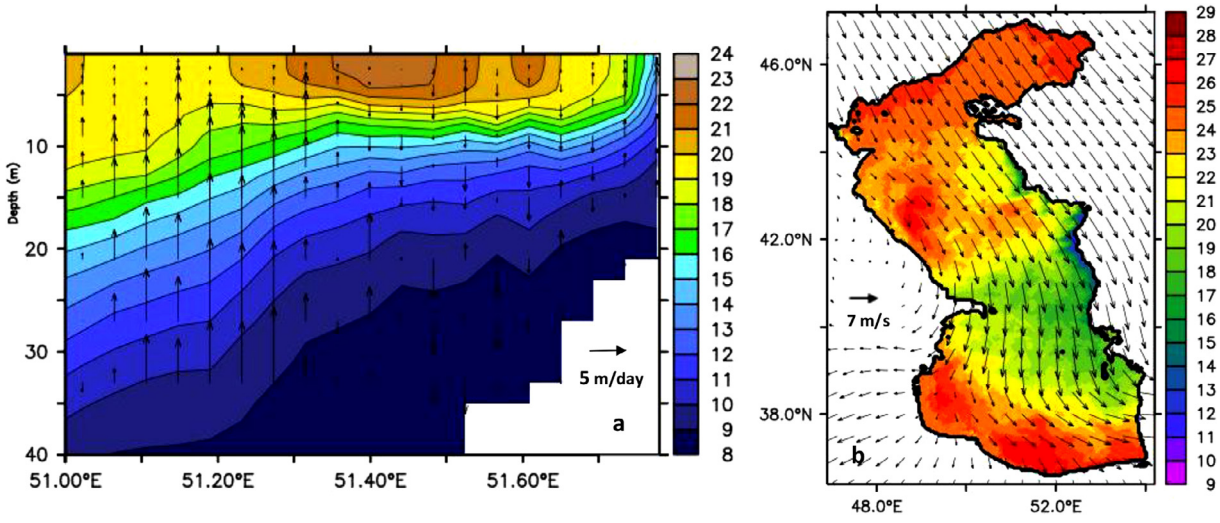

Figure 12 Vertical velocity over the vertical section of seawater temperature (°C) at 43°N (a) and SST (°C) with wind field overlaid (b) in the Caspian Sea on July 22.

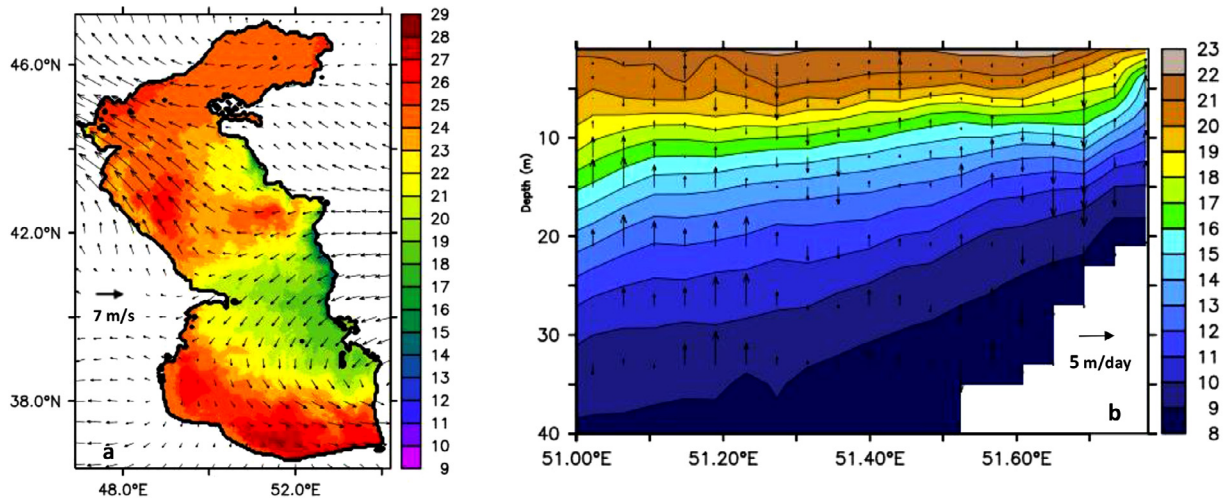

Figure 13 Vertical velocity over the vertical section of seawater temperature (°C) at 43°N (a) and SST (°C) with wind field overlaid (b) in the Caspian Sea on August 4.

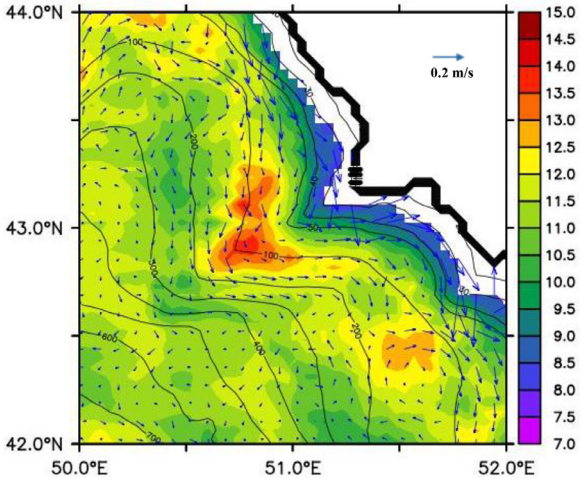

Figure 14 Plan view of the topography and model current vectors at a depth of 27 m and its seawater temperature (°C) in the eastern part of the middle Caspian Basin on August 4.

the eastern coast of the southern basin and the offshore area is noticeable in May. Upwelling occurs in upper layers at the 20 m depth to the surface and 15 km from the coast, which can be due to the wind field effect. However, in the middle Caspian basin, a slight upwelling occurs in lower layers, owing to the topographic effect. In June, in the middle basin, upwelling occurs within 25 km from the coast in upper layers at a depth of 35 m. Although the difference in SST (between coastal and offshore waters) in these two basins is negligible, the vertical temperature gradient is much more intense in the middle basin (43°N) than in the southern basin (39°N). Upwelling in the middle basin occurred 6, 4, and 4 times per month in June, July, and August, respectively, so that its intensity in June and July is much higher than in August. According to the wind field direction, upwelling events in June and July are mainly due to wind field effects and in August due to the bottom topography. In July and August, the mean of the maximum vertical velocities in the middle Caspian basin was estimated 10.58 m/day and 7.98 m/day, respectively, being in good agreement with the results obtained by Shia and Bidokhti (2015) (12 m/day and 7 m/day, respectively). The reason for the slight difference in these values can be explained by the difference in the forcing applied to the model. Wind-driven upwelling in August occurs in the eastern coasts of the middle Caspian basin within 25 km from the coast up to a depth of 15 m. The mechanism of upwelling formation in the middle Caspian basin in June and July is north or northeast wind (parallel to the coastline), being consistent with the results obtained by Knysh et al. (2008) indicating that the reason of upwelling in July is the prevailing wind from north to south in the middle Caspian basin. According to east and southeast winds in August and September in the eastern part of the middle basin, the upwelling in these months can be due to the effect of the bottom topography.

Declaration of competing interest

The authors declare that they have no known competing financial interests or personal relationships that could have appeared to influence the work reported in this paper.

References

Anand, P., Issac, P., Raghunadha Rao, A., 2019. Observed Interannual Variability of upwelling characteristics during 2016—2017: A Study using Princeton Ocean Model. Defence Sci. J. 69 (2), 142—148. https://doi.org/10.14429/dsj.69.14218

Antonov, J.I., Locarnini, R.A., Boyer, T.P., Mishonov, A.V., Garcia, H.E., Levitus, S., 2006. World Ocean Atlas 2005, vol. 2: Salinity. NOAA Atlas NESDIS, 62(2). NOAA: [s.l.], 182 pp.

Arpe, K., Tsuang, B.-J., Tseng, Y.-H., Liu, X.-Y., Leroy, S.A.G., 2018. Quantification of climatic feedbacks on the Caspian Sea level variability and impacts from the Caspian Sea on the large-scale atmospheric circulation. Theor. Appl. Climatol. 136 (1—2), 475—488.

Blumberg, A.F., Mellor, G.L, 1987. A Description of a Three-Dimensional Coastal Ocean Circulation Model. In: Heaps, N.S. (Ed.), Coastal and Estuarine Sciences, Book 4. Am. Geophys. Union, 1—6. https://doi.org/10.1029/CO004p0001

Bohluly, A., Sadat Esfahani, F., Montazeri Namin, M., Chegini, F., 2018. Evaluation of wind induced currents modeling along the Southern Caspian Sea. Cont. Shelf Res. 153, 50—63. https://doi.org/10.1016/j.csr.2017.12.008

Brink, K.H., 1983. The near-surface dynamics of coastal upwelling. Progr. Oceanogr. 12 (3), 223—257. https://doi.org/10.1016/0079-6611(83)90009-5

Closset, I., McNair, H.M., Brzezinski, M.A., Krause, J.W., Thamatrakoln, K., Jones, J., 2021. Diatom response to alterations in upwelling and nutrient dynamics associated with climate forcing in the California current system. Limnol. Oceanogr. 66, 1578—1593. https://doi.org/10.1002/lno.11705

Dumont, H.J., 1998. The Caspian lake: History, biota, structure, and function. Limnol. Oceanogr. 43 (1), 44—52.

Ghaffari, P., Isachsen, P.E., LaCasce, J.H., 2013. Topographic effects on current variabilityin the Caspian Sea. J. Geophys. Res.-Oceans, 118 (12), 7107—7116. https://doi.org/10.1002/2013JC009128

Gunduz, M., Özsoy, E., 2014. Modelling seasonal circulation and thermohaline structure of the Caspian Sea. Ocean Sci. 10 (3), 459—471. https://doi.org/10.5194/os-10-459-2014

Hall, J.K., 2002. Bathymetric compilations of the seas around Israel 1: The Caspian and Black Seas. GSI Current Res. 13, 105—108.

Ibrayev, R.A., Özsoy, E., Schrum, C., Sur, H.I., 2010. Seasonal variability of the Caspian Sea three-dimensional circulation, sea level and air-sea interaction. Ocean Sci. 6 (1), 311—329. https://doi.org/10.5194/os-6-311-2010

Kämpf, J., Chapman, P., 2016. Upwelling systems of the world. Springer Int. Pub., Switzerland, XV, 433 pp. https://doi.org/10.1007/978-3-319-42524-5

Kämpf, J., Sadrinasab, M., 2006. The circulation of the Persian Gulf: a numerical study. Ocean Sci. 2, 27—41. https://doi.org/10.5194/os-2-27-2006

Kara, A.B., Wallcraft, A.J., Metzger, E.J., Gunduz, M., 2010. Impacts of freshwater on the seasonal variations of surface salinity and circulation in the Caspian Sea. Cont. Shelf. Res. 30 (10—11), 1211—1225. https://doi.org/10.1016/j.csr.2010.03.011

Kitazawa, D., Yang, J., 2012. Numerical analysis of water circulation and thermohalinestructures in the Caspian Sea. J. Mar. Sci. Technol. 17 (2), 168—180. https://doi.org/10.1007/s00773-012-0159-0

Knysh, V.V., Ibrayev, R.A., Korotaev, G.K., Inyushina, N.V., 2008. Seasonal variability of climatic currents in the Caspian Sea reconstructed by assimilation of climatic temperature and salinity into the model of water circulation. Izv. Atmos. Ocean Phys. 44 (2), 236—249. https://doi.org/10.1134/S0001433808020114

Kosarev, A.N., Yablonskaya, E.A., 1994. The Caspian Sea. SPB Academic publisher, Russia, 259 pp.

Kostianoy, A., Kosarev, A., 2005. The Caspian Sea environment. Springer, Berlin, XIV, 272 pp. https://doi.org/10.1007/b138238

Lavrova, O.Y., Kostianoy, A.G., Lebedev, S.A., Mityagina, M.I., Ginzburg, A.I., Sheremet, N.A., 2011. Complex satellite monitoring of the Russian seas. Space Research Institute of RAS, Moscow.

Li, Y., Peng, S., Wang, J., Yan, J., Huang, H., 2018. On the mechanism of the generation and interannual variations of the summer upwellings west and southwest off the Hainan Island. J. Grophus. Res.-Oceans, 123, 8247—8263. https://doi.org/10.1029/2018JC014226

Mansoury, M., Sadrinasab, M., Akbarinasab, M., 2015. Modeling of salinity and temperature field structure in the Caspian Sea using POM model. Hydrophysics 1 (1), 1—13.

Medvedev, I.P., Kulikov, E.A., Fine, I.V., 2020. Numerical modelling of the Caspian Sea tides. Ocean Sci. 16, 209—219. https://doi.org/10.5194/os-16-209-2020

Mellor, G.L., Blumberg, A.F., 1985. Modeling vertical and horizontal diffusivities with the sigma coordinate system. Mon. Weather Rev. 113 (8), 1379—1383. https://doi.org/10.1175/1520-0493(1985)113<1379:MVAHDW>2.0.CO;2

Meunier, T., Rossi, V., Morel, Y., Carton, X., 2010. Influence of bottom topography on an upwellingcurrent: Generation of Long Trapped Filaments. Ocean Model. 35 (4), 277—303. https://doi.org/10.1016/j.ocemod.2010.08.004

Nigam, T., Pant, V., Prakash, K.R., 2018. Impact of Indian Ocean dipole on the coastal upwelling features off the southwest coast of India. Ocean Dynam. 68, 663—676. https://doi.org/10.1007/s10236-018-1152-x

Oey, L., Chang, Y.L., Lin, Y.C., Chang, M.C., Xu, F., Lu, H.F., 2013. ATOP-The Advanced Taiwan Ocean Prediction System Based on the mpiPOM. Part 1: Model Descriptions, Analyses and Results. Terr. Atmos. Ocean Sci. 24 (1), 137—158. https://doi.org/10.3319/TAO.2012.09.12.01(Oc)

Olita, A., Ribotti, A., Fazioli, L., Perilli, A., Sorgente, R., 2013. Surface circulation and upwelling in the Sardinia Sea: A numerical study. Cont. Shelf Res. 71, 95—108. https://doi.org/10.1016/j.csr.2013.10.011

Sadrinasab, M., Kämpf, J., 2004. Three dimensional flushing times of the Persian Gulf. Geophys. Res. Lett. 31, L24301. https://doi.org/10.1029/2004GL020425

Shanks, A.L., Largier, J., Brink, L., Brubaker, J., Hooff, R., 2000. Demonstration of the onshore transport of larval invertebrates by the shoreward movement of an upwelling front. Limnol. Oceanogr. 45 (1), 230—236. https://doi.org/10.4319/lo.2000.45.1.0230

Shiea, M., Bidokhti, A.A., 2015. The Study of upwelling phenomenon in the eastern coasts of the Middle Caspian basin using numerical simulation. Earth Space Phys. 41 (3), 535—545. https://doi.org/10.22059/jesphys.2015.55105

Shiea, M., Chegini, V., Bidokhti, A.A., 2016. Impact of wind and thermal forcing on the seasonal variation dimensional circulation in the Caspian Sea. Indian J. Geo-Mar. Sci. 45 (5), 671—686.

Su, J., Pohlmann, T., 2009. Wind and topography influence on an upwelling system at the eastern Hainan coast. J. Geophys. Res. 114, C06017. https://doi.org/10.1029/2008JC005018

Sun, Y.-J., Jalon-Rojas, I., Wang, X.H., Jiang, D., 2017. Coastal upwelling by wind-driven forcing in Jervis Bay, New South Wales: A numerical study for 2011. Estuar. Coast. Shelf. Sci. 206, 101—115. https://doi.org/10.1016/j.ecss.2017.11.022

Sur, H.I., Özsoy, E., Ibrayev, R., 2000. Satellite-derived flow characteristics of the Caspian Sea. In: Elsevier Oceanography Series, Vol. 63, 289—297.

Turuncoglu, U.U., Giuliani, G., Elguindi, N., Giorgi, F., 2013. Modeling the Caspian Seaand its catchment area using a coupled regional atmosphere-ocean model (RegCM4-ROMS): model design and preliminary results. Geosci. Model Dev. 6, 283—299. https://doi.org/10.5194/gmd-6-283-2013

Tuzhilkin, V.S., Kosarev, A.N., 2005. Thermohaline structure and general circulation of the Caspian Sea waters. In: Kostianoy, A.G., Kosarev, A.N. (Eds.), The Caspian Sea Environment, The Handbook of Environmental Chemistry, vol. 5P. Springer, Berlin, Heidelberg, 33—57. https://doi.org/10.1007/698_5_003

UNESCO-IHP-IOC-IAEA, 1996. Workshop on sea level rise and multidisciplinary studies of environmental processes in the Caspian region, IOC workshop No 108. 9—12 May, Paris, France.

Wirasatriya, JA., Setiawan, J.D., Sugianto, D.N., Rosyadi, I.A., Haryadi, H., Winarso, G., Setiawan, R.Y., Susanto, R.D., 2020. Ekman dynamics variability along the southern coast of Java revealed by satellite data. Int. J. Remote Sens. 41 (21), 8475—8496. https://doi.org/10.1080/01431161.2020.1797215

Zereshkian, S., Mansoury, D., 2020. Evaluation of ocean thermal energy for supplying the electric power of offshore oil and gas platforms. J. Earth Space Phys. 46 (2), 331—345. https://doi.org/10.22059/jesphys.2020.289441.1007161